

Aerodynamic Performance and Flow Characteristics of the 2D NACA 2412 Airfoil Using CFD

Yuchen Guo

Department of Mechanical and Aerospace Engineering, Rutgers New Brunswick, New Brunswick, USA

projason1234@gmail.com

Abstract. the Lift on a cambered airfoil depends on the interaction of pressure, vorticity, and the boundary layer. Classical inviscid flow theory alone cannot describe this process completely. In real flow conditions, viscosity becomes significant. The way circulation develops therefore influences the aerodynamic loading on the airfoil surface. Previous research has examined vortex behavior near the trailing edge. Liu's review points out that the starting vortex helps satisfy the Kutta condition and allows circulation to form. Other studies compare lifting-surface approaches with CFD methods. These works show that geometric features, such as camber and thickness, lead to nonlinear pressure effects. Simplified potential-flow models often struggle to predict these effects accurately. This study uses CFD to investigate the NACA 2412 airfoil at a Reynolds number of approximately 3.1×10^6 . A C-type computational domain is applied with a structured quadrilateral mesh. The mesh maintains a near-wall resolution of $y^+ \approx 1$, which enables reliable boundary-layer resolution. The pressure, velocity, and streamline results display clear suction peaks and smooth pressure recovery. The flow field also shows stable circulation around the airfoil. The numerical results agree well with available experimental data. Similar trends appear in Reynolds-number sensitivity and boundary-layer stability reported in earlier studies. This analysis demonstrates that CFD provides an effective connection between aerodynamic theory and real flow behavior.

Keywords: Aerodynamics, Airfoil, Computational Fluid Dynamics (CFD), NACA 2412

1. Introduction

Airfoil aerodynamics combines theoretical modeling with experimental observation. Potential-flow theory provides a clear description of inviscid lift generation, but real aerodynamic behavior involves more than ideal flow assumptions. Viscosity and boundary-layer effects play important roles in practical conditions. Flow separation and circulation development also influence how lift is produced. Previous studies show that lift formation depends strongly on vorticity near the trailing edge. Liu's review explains that vorticity generation, starting vortex formation, and boundary-layer shear control how circulation is established in real flows [1]. These mechanisms explain the pressure

reduction on the upper surface and the resulting lift, which goes beyond simplified explanations based only on velocity differences.

Accurate prediction of airfoil behavior is essential for many engineering systems, including small UAVs, general aviation aircraft, and wind-energy devices. Their performance depends on reliable estimates across different Reynolds numbers and turbulence levels. Research comparing lifting-surface models with high-fidelity CFD reveals clear limitations in simplified approaches. These models often fail to capture the effects of airfoil thickness, camber, or morphing deflections, especially in regions dominated by nonlinear pressure gradients [2]. For cambered airfoils such as the NACA 2412, geometric features strongly influence pressure distribution. They shift suction peak locations, affect pressure recovery, and alter trailing-edge loading. Due to this sensitivity, CFD provides a more suitable tool for analyzing airfoil behavior under realistic flow conditions.

Numerical studies of NACA profiles have demonstrated that CFD can replicate the development of lift and drag with strong correlation to wind-tunnel results, if turbulence modeling and near-wall resolution are handled properly [3]. Additional insights from research on Reynolds-number effects indicate that laminar–turbulent transition, separation bubbles, and turbulence intensity can influence the slope of the lift curve and the onset of stall [4]. Spoiler and circulation-focused studies further show how flow turning, vorticity sheets, and wake deflection contribute to momentum-based explanations for lift and control effectiveness [5]. Lastly, research on wall-resolution strategies highlights the importance of maintaining y^+ values near unity for accurate shear-stress and pressure-gradient prediction near solid boundaries, especially in high-Reynolds-number external flows [6].

The present study applies these principles to the NACA 2412 airfoil using a CFD approach designed to capture relevant viscous and inviscid behavior. The objective is to visualize the aerodynamic mechanisms that established theory and recent research describe, and to interpret CFD-based pressure, velocity, and streamline results within this broader scientific framework.

2. Methods and results

Airfoil geometry and domain configuration: The NACA 2412 profile was generated with 200 coordinate points to preserve curvature accuracy, particularly near the leading edge where geometric errors can distort stagnation behavior. A chord length of 1 m was used for normalization. A C-type computational domain was then constructed following established best practices for external airfoil simulation. The upstream semicircular boundary extended 7.5 m from the leading-edge center, while a 15 m rectangular wake region was placed downstream. This configuration helps minimize boundary interference and supports stable convergence when solving steady-state RANS equations. Two vertical refinement lines located at the trailing edge and 80 mm upstream were introduced to distribute mesh density more effectively around the airfoil [7].

Mesh Generation and Boundary-Layer Strategy: For the mesh sizing procedure, the inlet line along the x-axis, the two vertical lines, and the two outlet lines were each assigned approximately 250 divisions with a bias factor of 50,000. This configuration concentrates elements near the airfoil surface compared to the outer boundaries of the domain. The line along the x-axis downstream of the trailing edge and the two-horizontal outer-domain lines were set to 150 divisions with hard behavior and a bias factor of 300. In addition, both the upper and lower airfoil surfaces were discretized with 150 divisions. The inlet of the C-shaped domain and the leading-edge region were assigned 100 divisions. A face size control was finally applied to generate a quadrilateral-dominant mesh. The resulting mesh is shown in Figure 1 below.

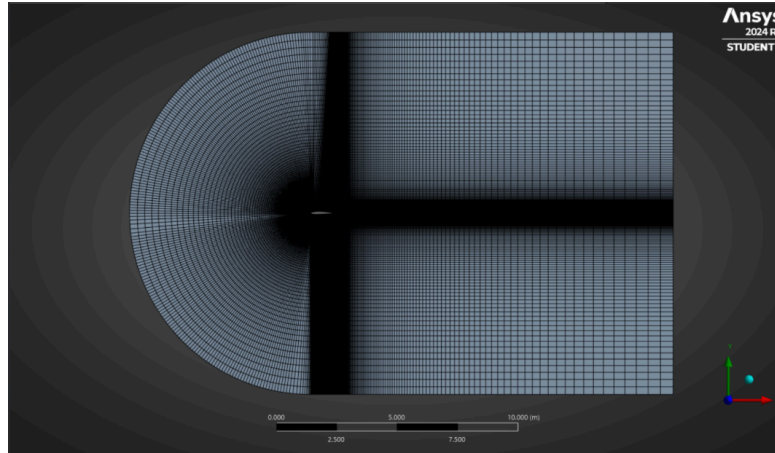


Figure 1. Meshing boundary and domain size

From the mesh refinement near the airfoil, the cell volume transitions significantly from the leading edge to the trailing edge, and some skewness appears in this region. In the final report, the vertical extent upstream of the leading edge will be reduced—likely to less than 80 mm—to mitigate this issue and improve orthogonality.

A critical aspect of the mesh evaluation is the wall-resolution requirement quantified by the non-dimensional parameter y^+ (y-plus). This parameter indicates how well the first-layer cell height resolves the viscous sublayer. To accurately capture near-wall viscous effects, a target value of $y^+ \approx 1$ is required. Beyond $y^+ \approx 10^0$, the dimensionless velocity U^+ enters a non-linear regime [6]. The wall-function behavior is expressed as:

$$\text{viscous sublayer } y^+ < 5, \quad u^+ = y^+ \quad (1)$$

As the y^+ value influences the wall-pressure gradient and the separation characteristics along the airfoil, maintaining $y^+ < 1$ is essential. For the NACA 2412 airfoil, a Reynolds number of approximately 3.1×10^6 was selected under standard conditions at the air temperature is 15 degrees Celsius. The corresponding velocity-profile behavior is illustrated in Figure 2.

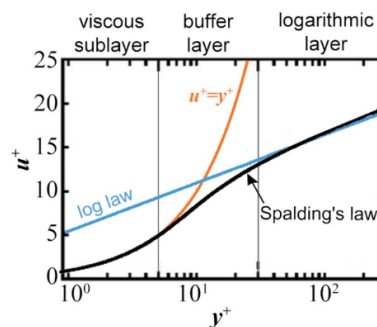


Figure 2. Wall function [6]

$$Re = \frac{\rho u L}{\mu} \quad (2)$$

$$\text{at } T = 15 \text{ }^\circ\text{C}, \quad \rho = 1.225 \frac{\text{kg}}{\text{m}^3}, \quad \mu = 1.802 \times 10^{-5}, \quad \text{set } L = 1\text{m} \quad (3)$$

$$u = \frac{Re \times \mu}{uL} \approx 45.6\text{m/s} \quad (4)$$

With this information we could calculate the first cell height from y^+ calculator as around 0.016889604 mm [8].

Using the mesh resolution near the airfoil surface, the boundary-layer thickness is measured to be approximately 6.32×10^{-3} mm, as shown in Figure 3. Since this value is smaller than the required first-cell height of 0.016889604 mm, the resulting y^+ remains within an acceptable range [6]. Therefore, the mesh meets the near-wall resolution criteria for accurate boundary-layer modeling.

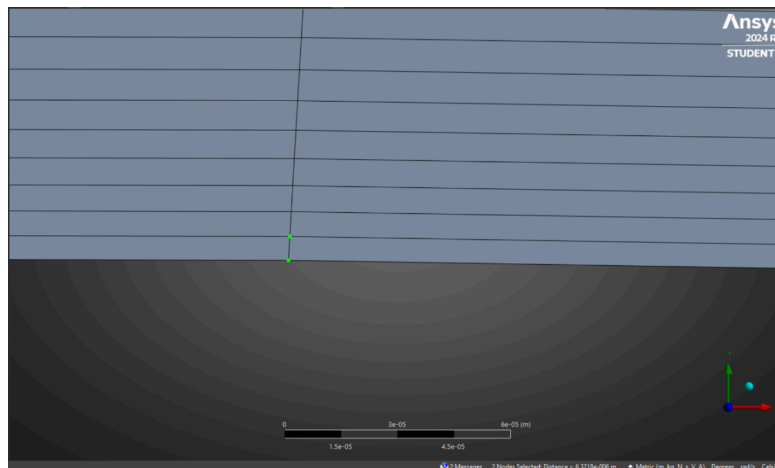


Figure 3. Boundary layer thickness

Pressure Distribution: The pressure field shows the classical characteristics of a cambered airfoil operating at moderate Reynolds number. A strong suction peak forms immediately downstream of the leading edge on the upper surface, consistent with the curvature-induced acceleration predicted by inviscid theory while remaining tied to viscous enforcement of the Kutta condition as described by Liu [1]. The pressure gradually recovers toward the trailing edge, forming an adverse pressure gradient that influences boundary-layer thickness but remains mild enough to prevent significant separation at the simulated condition. The stagnation region at the leading edge is clearly visible on the lower surface, accompanied by a region of elevated static pressure that contributes to lift.

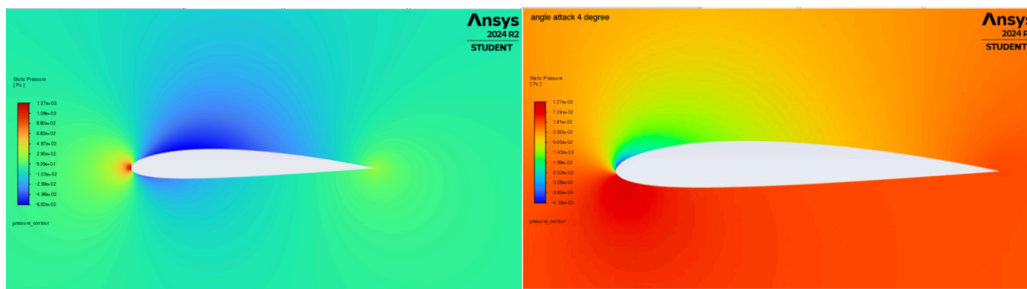


Figure 4. Pressure contour for NACA 2412 airfoil (zero & four degrees AOA)

Velocity Distribution: The velocity contour shows accelerated flow over the upper surface of the airfoil. Geometric camber and local pressure gradients drive this acceleration. The highest velocities occur in regions with strong suction, which align closely with the pressure minimum along the upper surface. This relationship confirms the link between pressure reduction and increased flow speed. The accelerated flow is associated with the circulation that produces lift, as reported in both theoretical and experimental studies [1,3]. On the lower surface, flow velocities remain lower along most of the chord. Near the trailing edge, the flow begins to recover. The boundary layer stays attached, and the wake remains narrow. These features indicate stable flow at the selected Reynolds number and agree with previous findings on Reynolds-number sensitivity and lift-curve behavior [4].

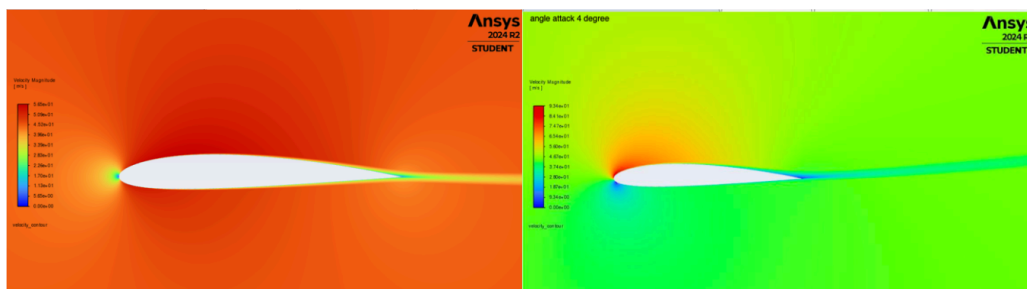


Figure 5. Velocity contour (m/s), flow around airfoil (zero & four degrees AOA)

Streamline behavior: Streamlines and velocity vectors illustrate the development of circulation and wake structure around the airfoil. The flow curves tightly near the leading edge and merges smoothly at the trailing edge, which satisfies the Kutta condition. The wake shows a slight downward deflection, indicating that the airfoil transfers downward momentum to the flow. This behavior supports the momentum-based explanation of lift reported in previous circulation and spoiler studies [5]. Velocity vectors are densely packed above the upper surface, where shear and flow acceleration are strong. Below the airfoil, vectors are slower and more widely spaced, which reflects higher pressure in that region. The resulting circulation pattern matches both theoretical expectations and earlier CFD results for the NACA 2412 airfoil [3].

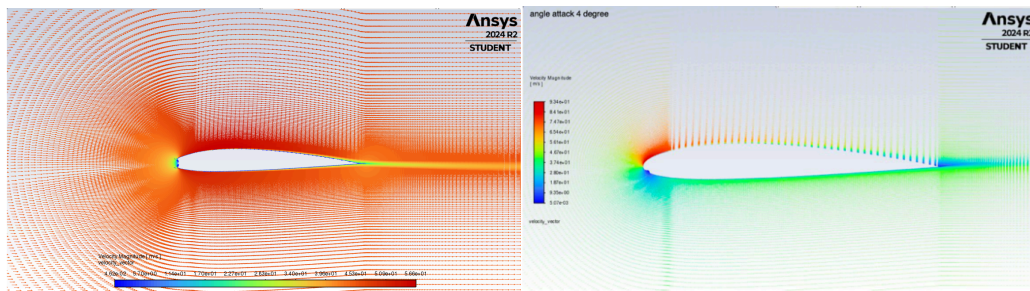


Figure 6. Velocity-vector field and streamlines (zero- & four-degrees AOA)

Integrated Interpretation of Flow Physics: The pressure, velocity, and streamline results together provide a clear picture of the aerodynamic behavior. The strong suction peak and accelerated flow over the upper surface support classical lift mechanisms. At the same time, these features show the influence of viscous and vorticity-driven effects described in modern aerodynamic studies [1]. The pressure gradient along the surface remains mild, and the boundary layer stays attached. This behavior reflects Reynolds-number effects related to flow stability and transition reported in previous research [4]. The circulation seen in the streamline plot also matches observations from spoiler-based flow-turning studies, where downward wake deflection is directly linked to lift production [5]. Overall, the CFD results capture the key flow features reported in earlier experimental and numerical studies of NACA-series airfoils [3].

3. Conclusion

This study used CFD to analyze the aerodynamic behavior of the NACA 2412 airfoil, focusing on pressure, velocity, and streamline development under moderate Reynolds-number conditions. The resulting flow fields align with both classical theoretical concepts and modern research describing viscous-flow mechanisms, circulation establishment, and boundary-layer evolution. The cambered geometry of the NACA 2412 produces strong suction and accelerated flow over the upper surface, creating circulation in agreement with Liu's theoretical synthesis and with experimental CFD-based findings.

The comparison between numerical predictions and established research further highlights the importance of capturing geometric effects, as lifting-surface approximations can miss nonlinear pressure distributions that CFD resolves effectively. The behavior of the boundary layer and pressure recovery also tracks well with studies examining Reynolds-number sensitivity and transition effects. In addition, wake deflection patterns support momentum-based interpretations of lift as discussed in circulation and spoiler-related literature. Finally, the successful use of $y^+ \approx 1$ mesh resolution demonstrates the value of direct viscous-sublayer modeling, consistent with near-wall modeling recommendations from recent computational studies.

Overall, the simulation confirms CFD as a powerful tool for linking theoretical aerodynamic frameworks with practical flow physics and offers a detailed visualization of the mechanisms responsible for lift on the NACA 2412 airfoil.

References

- [1] Liu T (2021) Evolutionary understanding of airfoil lift. *Advances in Aerodynamics*.
- [2] Xu H, et al. (2022) Comparative study of lifting surface and CFD methods in morphing-wing simulation. *International Journal of Aerospace Engineering*.
- [3] Chandravadan N (2024) Numerical study of flow over NACA 2412 airfoil at various AOAs. *IJSRET*.

- [4] Michna J and Rogowski K (2022) Effect of Reynolds number and turbulence intensity on NACA 0018. Processes, 10: 1004.
- [5] Hoque A, et al. (2024) Circulation and vorticity around a supersonic airfoil with a spoiler. Aerospace Systems.
- [6] Han M, Ooka R, Kikumoto H (2021) Wall-function approach in lattice Boltzmann method. Fluid Dynamics Research, 53: 045506.
- [7] Airfoil Tools. (n.d.). NACA 4-digit airfoil search. Retrieved November 29, 2025, from <http://airfoiltools.com/search/index?m%5Bgrp%5D=naca4d& m%5Bsort%5D=1>
- [8] Volupe. (2023). All y+ calculator – when meshing a geometry for CFD analysis. Retrieved from <https://volute.com/support/all-y-calculator-when-meshing-a-geometry-for-cfd-analysis/>

Appendix

The NACA 2412 airfoil data:

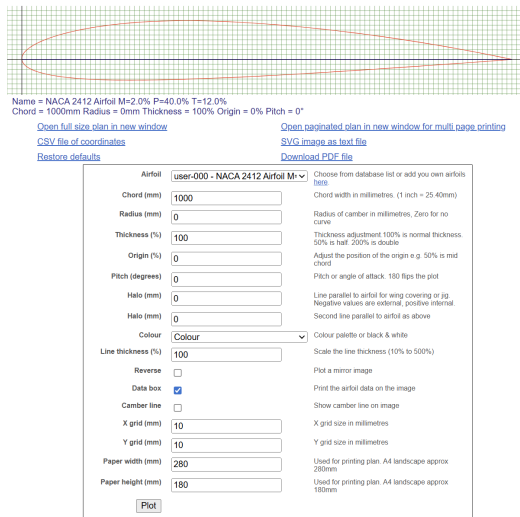


Figure A. NACA2412 airfoil sizing detail

The way to calculate the first cell height from y+ calculator as around 0.016889604 mm:

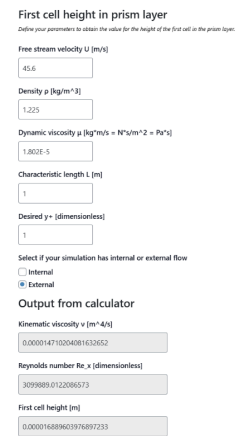


Figure B. Y+ calculator CFD [8]

Meshing detail around the airfoil is shown:

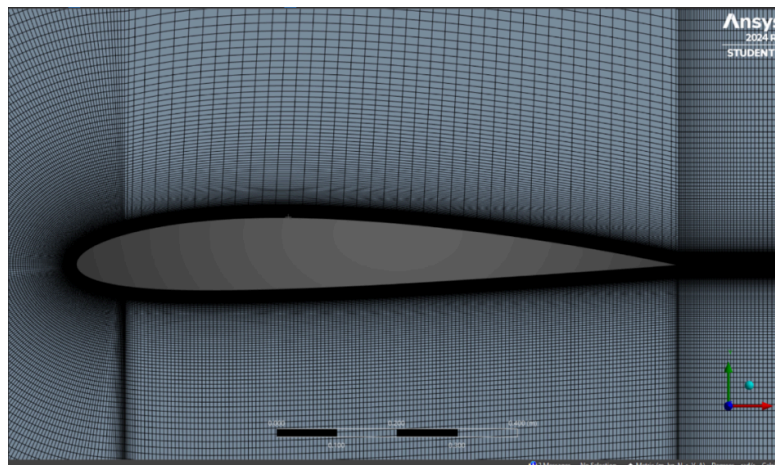


Figure C. Meshing detail